International Journal of Electrochemical Science 18 (2023) 100109

Contents lists available at ScienceDirect

International Journal of Electrochemical Science

journal homepage: www.journals.elsevier.com/ijoes

Hydrothermal synthesis of GO/ZnO composites and their micromorphology and electrochemical performance

Sugianto Sugianto[a,*], Budi Astuti[a], Endah F. Rahayu[b], Triastuti Sulistyaningsih[b], Nabila Yasiroh[b], Irma F. Yanti[b], Didik Aryanto[c]

[a] Department of Physics, Faculty of Mathematics and Natural Sciences, Universitas Negeri Semarang, Jl. Raya Sekaran, Gunungpati 50299, Indonesia
[b] Department of Chemistry, Faculty of Mathematics and Natural Sciences, Universitas Negeri Semarang, Jl. Raya Sekaran, Gunungpati 50299, Indonesia
[c] Research Center for Advance Materials, Badan Riset dan Inovasi NasionalSerpong 15314, Tangerang Selatan, Banten, Indonesia

ARTICLE INFO

Keywords:
Composite
Electrochemical performance
Graphene oxide
Micromorphology
ZnO nanorods

ABSTRACT

In this study, a graphene oxide/zinc oxide (GO/ZnO) composite was synthesized by the one-pot hydrothermal technique using various GO/ZnO ratio compositions. These were characterised by scanning electron microscopy (SEM), Fourier-transform infrared (FTIR) and Raman spectroscopy. The findings reveal that the GO/ZnO composite has three different micromorphologies: ZnO-nanorods (ZnO-NRs) were embedded and agglomerated over the GO surface; ZnO-microrods (ZnO-uRs) adhered to and separated on the GO surface; and GO was coated by ZnO at 1:1, 1:2 and 1:8 ratios. In addition, the electrochemical performance of the synthesized GO/ZnO composites was investigated using cyclic voltammetry (CV). The results show that the embedded and agglomerate of ZnO-NRs over the GO surface have the best performance, indicated by a larger CV curve area and higher specific capacitance than the GO and other GO/ZnO composites. The results indicate that the incorporation and insertion of GO and ZnO NRs have an effective reversible nature and are promising electrode materials for supercapacitor applications.

1. Introduction

Over the past decade, global environmental issues, such as global warming and the depletion of fossil energy, have inspired extensive research into the development of various eco-friendly renewable energy devices. Such devices are considered to be among the solutions to the problem. Supercapacitors are becoming the candidate with the most potential as an energy storage device. This is because of their higher power density, long cycle lifetime, and lower maintenance cost than batteries [1–3]. Moreover, they have a shorter charge time and higher specific energy density than conventional capacitors [1]. Electrochemical double-layer capacitance (EDLC) and pseudo-capacitance are two supercapacitor types distinguished by the charge-storage mechanism. The capacitance of EDLC comes from electrostatic charge diffusion, which accumulates at the electron-electrolyte interface [4,5]. Usually, materials with a high surface area and excellent electrical conductivity are selected. Carbon-based materials are the most suitable choice, which encourage the use of various forms of EDLC electrodes. However, their low specific capacitance severely limits their subsequent application [4]. As an alternative, pseudo-capacitors with Faradaic storage mechanisms and which store the charge according to rapid and reversible redox reaction [4,6], can provide much higher capacitance and energy density. Transition metal oxides, metal hydroxides and polymeric materials have been explored for pseudo-capacitor applications [5]. The results indicate that the best pseudo-capacitor property is exhibited by ruthenium oxide (RuO_2) [5,7]. However, the material is not very attractive for large-scale production because of its high cost, limited availability, and the fact that it is not environmentally friendly. ZnO is a metal oxide semiconductor with a wide band-gap, specific energy density, excellent oxide ionic conductivity, and relatively high power and capacity [4,8]. Moreover, it is non-toxic, low cost, eco-friendly and has abundant availability [9]. This makes ZnO a potential material for supercapacitors as a replacement for RuO_2.

Based on the advantages and disadvantages of the two types of capacitors, many studies have considered capacitors based on a combination of carbon materials with pseudocapacitive behaviour. ZnO-carbon material hybrids have become one of the choices. The bonding of ZnO with the carbon materials can improve the electron chemical

* Corresponding author.
E-mail addresses: sugianto@mail.unnes.ac.id, sugiantomipa@gmail.com (S. Sugianto).

https://doi.org/10.1016/j.ijoes.2023.100109
Received 19 December 2022
Available online 21 March 2023

and electrical conductivities of the out-site current collectors because of the synergistic effect produced by each another [10]. Kalpana et al. [1] reported that ZnO/carbon aerogel composite supercapacitors have a maximum capacitance of 500 F/g at 100 mA/cm^2 and that their specific capacitance is constant up to 500 cycles at all current densities (25, 50, 75, and 100 mA/cm^2). ZnO/active carbon nanocomposite supercapacitors have been studied by Selvakumar et al. [11] and Lee et al. [7]. Selvakumar et al. [11] argue that coating nanostructure ZnO onto active carbon as a specific capacitance of 160 F/g, which decreases with increased ZnO content. In comparison, Lee et al. [7] show the ZnO nanorod coating onto an active carbon surface with a specific capacitance value of 155 F/g. Another work by Fahimi and Moradlou [3] considered a ZnO/carbon foam supercapacitor with a specific capacitance of 1120 mF/cm at a current density of 4 mA/cm^2. A carbon nanotube/ZnO nanocomposite supercapacitor was also analyzed by Sinha et al. [12] and Otun et al. [6]. Their results demonstrate that the composite is promising for enhancing electrochemical energy storage performance. Structural analysis of ZnO/rGO hybrids has revealed a homogeneous distribution of ZnO nanorods inserted into the GO nanosheet with a high specific capacitance of 140 F/g, even at the scan rate of 500 mV/s, and long-term cycle stability (94 % capacitance retention over 2000 cycles) [4]. A ZnO/rGO nanocomposite supercapacitor with spherical particles of ZnO embedded in the GO sheet was also studied by Saranya et al. [2], Kalaiarasi et al. [13], Rai et al. [10], and Prabhuraj et al. [14]. Their results show a specific capacitance of 122.4 F/g [2], 345 F/g [10], and 293.5 F/g [14], with specific capacitance retention of over 80 %. These studies indicate that the relationship between the ZnO/GO composite microstructure and electrochemical properties in supercapacitor application still need further investigation.

This study focuses on synthesizing a GO/ZnO composites using a one-pot hydrothermal technique and their electrochemical performance. The various mass ratios of GO/ZnO in the synthesis process result from their different micromorphologies. This was confirmed by SEM imagery and supported by FTIR and Raman spectra. The influence of their micromorphologies on the electrochemical properties was investigated, with these shown to be closely related to the supercapacitor application.

2. Experimental

2.1. Materials

Graphite powder (Merck, Mr = 12.01 gr/mol), sulfuric acid 96 % (Merk, Mr = 98 gr/mol), phosphate acid 85 % (Emsure, Mr = 97.99 gr/mol), potassium permanganate (Merck, Mr = 158 gr/mol), zinc nitrate hexahydrate (Merk, reagent grade, 98 %), hydrochloric acid (Merck, ACS reagent, 37 %), $K_3[Fe(CN)_6]$ (Merck, Mr = 329.24 gr/mol) and KCl (Merck, Mr = 74.55 gr/mol) were employed. All the materials were used as received without any further purification.

2.2. Preparation of GO

Graphite oxide (GO) was prepared using a modified Hummer method with phosphate and sulfuric acid as oxidising agents. Sulfuric acid (90 mL) and phosphoric acid (10 mL) at a ratio of 9:1 were mixed and stirred for several minutes. 2 g of graphite powders were then added to the solution while stirring. Subsequently, 5 g of $KMnO_4$ was slowly added to the solution with constant stirring for 2 h to obtain the GO powder. 3 mL of H_2O_2 was then added to the mixture while stirring [15]. The GO was then washed with 10 mL of 10 % HCl with aquademin added to the solution [16], and then the solution was centrifuged for 15 min at a speed of 4500 rpm [15]. The suspension resulting from the centrifugation was then taken, aquademin added, and then centrifuged again. The washing process was repeated until the pH was neutral [17]. The GO suspension was then baked at a temperature of 110 ˚C for 3 h [18].

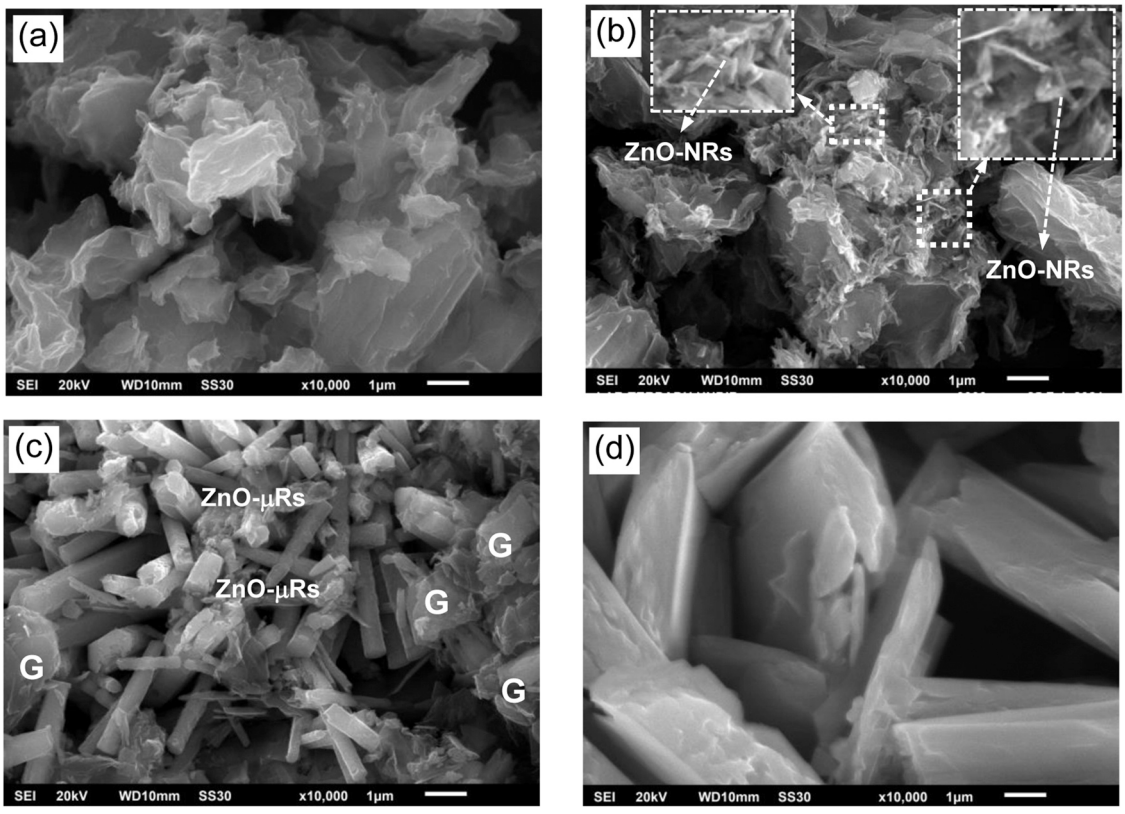

Fig. 1. SEM images of (a) GO, and GO/ZnO-composites with mass ratios of (b) 1:1, (c) 1:2, and (d) 1:8.

Table 1
Chemical composition of the GO/ZnO composite.

GO/ZnO mass ratio	Element (wt. %)			
	C	O	Zn	Total
1:1	74.13	18.09	7.78	100
1:2	40.75	35.73	23.52	100
1:8	15.92	40.11	43.97	100

2.3. Synthesis of GO/ZnO composite

The synthesis was performed with a mass ratio of GO:$Zn(NO_3)_2$. The mass ratio variations were 1:1 (0.2 g:0.2 g), 1:2 (0.2 g:0.4 g), and 1:8 (0.2 g:1.6 g), which were synthesized by the one-pot hydrothermal technique for 2 h. The GO solid was ultrasonicated for 1 h. The Zn $(NO_3)_2$ was then added according to the ratio with 10 mL N_2H_4, followed by ultrasonication for 30 min. The solution was transferred to an autoclave and placed in an oven at 160 ^{0}C for 2 h. The resulting GO/ZnO suspension was centrifuged at 4000 rpm for 15 min and then baked at 110 °C for 3 h.

2.4. Material characterisation

The GO/ZnO composite microstructure morphologies were investigated using scanning electron microscopy (SEM) equipped with an energy-dispersive X-ray spectroscopy (EDX) analyser. The Fourier-transform infrared spectroscopy (FT-IR) spectrum in a range of 400 – 4000 cm^{-1} was used to determine the functional group of the GO/ZnO composite. The material's lattice vibration was studied using a Raman spectrometer with monochromatic light from a laser source of wavelength 514 nm. The electrochemical properties of the GO/ZnO composite were studied by cyclic voltammetry (CV) measurement. A screen-printed carbon electrode (SPCE) was used for the electrochemical measurements. In the preparation of the GO/ZnO-SPCE, 1 mg of GO/ZnO was dissolved in 1 mL of aquademin (1:1). The suspension was then ultrasonicated for 20 min. The sonicated suspension was then dripped onto the working electrode on the SPCE and dried for 2 h. The dry GO/ZnO-SPCE electrode was then scanned using a 5 mmol/L $K_3[Fe(CN)_6]$ solution in 0.1 mol/L KCl.

3. Results and discussion

Fig. 1 presents the SEM microstructures of the GO and GO/ZnO composites with the ratios of 1:1, 1:2, and 1:8, respectively. Fig. 1(a) shows that the GO microstructure had a crumpled and wrinkle-like surface. This confirms that the results of the GO synthesis in this work show a distinctive characteristic of GO, as indicated by other reports [19,20]. The dark and wrinkled surface of the GO microstructure was caused by the accumulation of thick graphene sheets of oxygen functional groups and defects in the peeling process [21]. Fig. 1(b-d) show the SEM images of the 1:1, 1:2 and 1:8 ratios of GO/ZnO respectively. The GO/ZnO composite morphology is highly influenced by the level of ZnO addition in their synthesis. The SEM morphology reveals that ZnO nanorods (ZnO-NRs) were embedded and agglomerated over the GO surface at a similar ratio between GO and ZnO (1:1) (see Fig. 1(b)). The ZnO becomes microrods (μRs), which adhere to and separate (become independent) on the GO surface when the GO/ZnO composite is at a ratio of 1:2, as shown in Fig. 1(c). The formation of μRs occurred due to the higher concentration of Zn ions in the solution and contributed to the increasing growth rate of ZnO to rod structure with micro size. A very different result was produced by adding $Zn(NO_3)_2$ eight times, with ZnO-NRs and μRs not observed in the SEM morphology. It can be seen that the GO/ZnO composite has the form of a flake, which indicates that ZnO has coated the GO. In addition, an agglomerate between the GO and ZnO occurred during the synthesis.

The uniform coating of the $Zn(NO_3)_2$ solution over the graphene resulted in a strong nucleation reaction between ZnO and GO. The strong intermolecular forces allowed them to combine and grow together through physical or chemical adsorption. The results of this study are supported by previous work on the synthesis of ZnO/active carbon by Lee et al. [7]; the low concentration of zinc precursor solution formed a smaller ZnO nanostructure on the active carbon compared to the high concentration of zinc precursor solution. In addition, elemental quantitative analysis of the GO/ZnO composite was investigated using electron dispersive x-ray spectroscopy (EDX); the results are presented in Table 1.

The ratio of Zn and O was not equal in the GO/ZnO composite with compositions of 1:1 and 1:2, which indicates the presence of GO and ZnO in the sample. The ratio of Zn and O is almost equal, and the amount of C in the composite is lower than Zn and O, with a GO/ZnO ratio of 1:8. This indicates that the GO is coated and agglomerated with ZnO. In general, the amount of Zn and O elements increases, with the C element decreasing with the increasing level of ZnO in the GO/ZnO composite ratio. The results affirm that the level of ZnO increases in the GO/ZnO composite according to the increase in ZnO in the synthesis process.

The FTIR spectra of the GO and GO/ZnO composite with the mass ratios of 1:1, 1:2, and 1:8 are shown in Fig. 2. The characteristic IR features of GO in Fig. 2(a) show peaks at 1057 and 1707 cm^{-1}, corresponding to C-O bending and C═O stretching. The oxidation process of the graphite occurred in the synthesis of GO using Hummer's method, which generated oxygen functional groups [2]. In addition, a peak located at 1626 cm^{-1} contributes to the stretching vibration of the C═C bonding. Another peak at 3404 cm^{-1} reveals the COOH group because of OH and water molecules [13]. The GO/ZnO composite with different ratios is shown in Fig. 2(b-c). The oxygen functional groups at 1057, 1707 and ~3000 cm^{-1} were found to decrease, which indicates the reduction of GO (rGO) during the hydrothermal process [2,10]. The peak around 1384 cm^{-1} represent a stretching vibration of the C═O bond, which was attributed to vibration modes of the nitrate group [22,23] used as a precursor. In addition, the peaks corresponding to the vibration of the Zn-O bond at 420 and 568 cm^{-1} were also observed in the GO/ZnO composite with mass ratios of 1:2 and 1:8 (Fig. 2(c-d)).

The peak at 420 cm^{-1} in the 1:2 ratio came from ZnO-μRs, which adheres to and separates (becomes independent) on the GO surface. Unlike the 1:8 ratio, the appearance of the 568 cm^{-1} peaks confirms the incorporation of ZnO in the reduction of GO, as demonstrated by Rai et al. [10]. The results are also supported by previous reports on ZnO nanoparticles (NPs), in which the characteristic stretching mode of the Zn-O bond is in the range of 400 cm^{-1} to 500 cm^{-1} [24]. Another work by Handore et al. [25] shows the peak at 545 cm^{-1} as a stretching mode

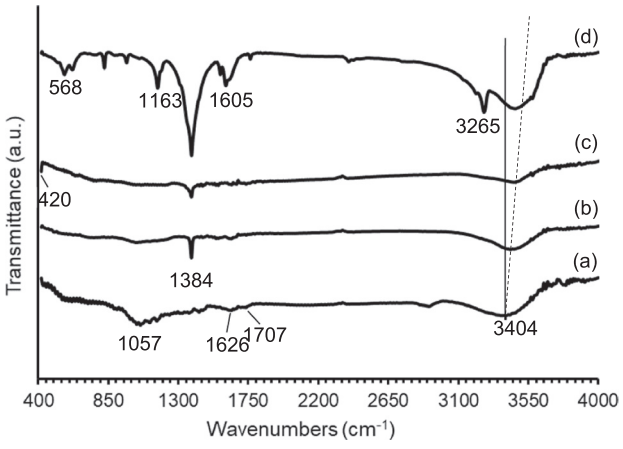

Fig. 2. FTIR spectra of (a) GO, and GO/ZnO-composites with mass ratios of (b) 1:1, (c) 1:2, and (d) 1:8.

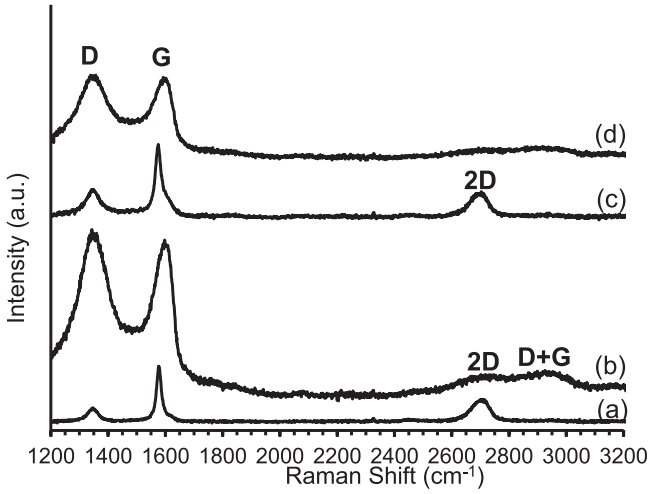

Fig. 3. Raman spectra of (a) GO, and GO/ZnO-composites at ratios of (b) 1:1, (c) 1:2, and (d) 1:8.

of the Zn-O bond. However, ZnO-NRs or -μRs were not observed on the GO surface or embedded within it. This confirms that neither ZnO-NRs or -μRs are formed during the hydrothermal process with higher concentrations of $Zn(NO_3)_2$, but that ZnO is evenly dispersed in GO and reacts with each other. The finding is confirmed by SEM images in Fig. 1(d). However, the peak of the Zn-O bond is not clearly seen in the FTIR spectra of the GO/ZnO composite with a 1:1 ratio (see Fig. 2(b)). The formation of ZnO-NRs embedded in the GO caused the peak of the Zn-O bond to decrease and is not clearly seen in the FTIR spectra.

The crystallisation, structural defects and disorders of GO and GO/ZnO-composite products were investigated by Raman spectroscopy, whose results as shown in Fig. 3. All the GO and GO/ZnO composite samples revealed the D-band and G-band at around 1347 and 1590 cm^{-1} respectively. The two characteristic bands of graphene-based material, i.e., the D and G bands, correspond to the sp^3 defect or disorder and sp^2 hybridised orbitals of the C-C bond [4,10,20,26]. A low intensity D-band and high intensity G-band (with an I_D/I_G intensity ratio of 0.26) were observed in the Raman spectra of GO, as shown in Fig. 3(a), which demonstrates the characteristic of graphene-base material. The results indicate that the C-C bond is more ordered and has a small mean size of the sp^2-domain in GO materials based on the synthesis of this study. The position and intensity of the D and G bands depend on many factors, such as defect, doping level etc.

Many previous reports show that defects in graphene can be seen depending on the ratio [10,26]. The findings of this research show that the I_D/I_G ratio for the GO/ZnO-composite with 1:1, 1:2, and 1:8 ratios are 1.06, 0.37 and 1.09 respectively. It is revealed that the defect in the GO materials was smaller than in the other samples when the GO/ZnO composite was at the 1:2 ratio. The few ZnO particle concentrations embedded in the GO may contribute in this case. In general, the formation of ZnO μRs during hydrothermal processes is separated or not embedded in GO. This is supported by higher and sharp G-band peaks on the Raman spectra, which corroborate the SEM results (Fig. 1(c)). Decoration of ZnO on GO during the hydrothermal process causes a

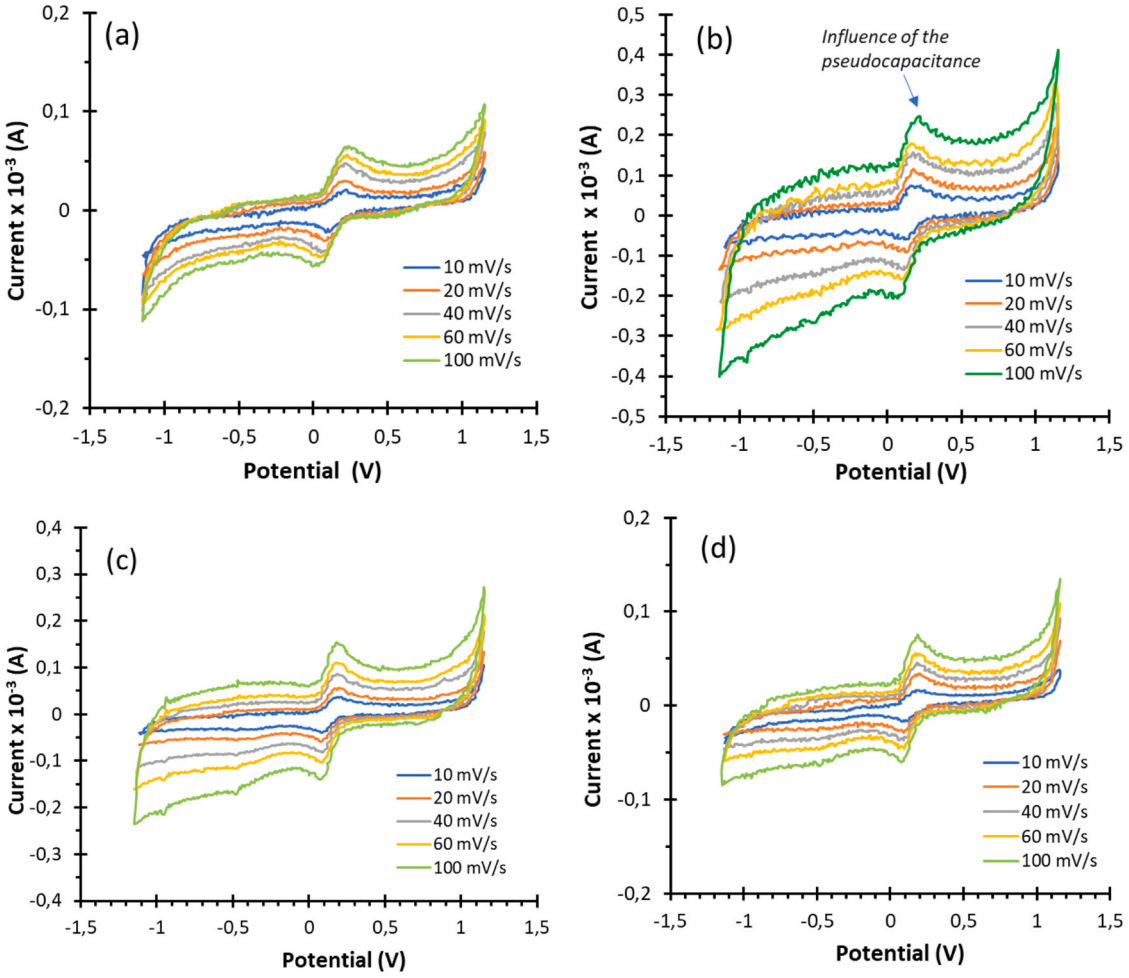

Fig. 4. CV curves of (a) GO, and GO/ZnO-composites with compositions of (b) 1:1, (c) 1:2, and (d) 1:8 at different scan rates (10, 20, 40, 60 and 100 mV/s) with 5 mmol/L $K_3[Fe(CN)_6]$ solution in 0.1 mol/L KCl as electrolyte.

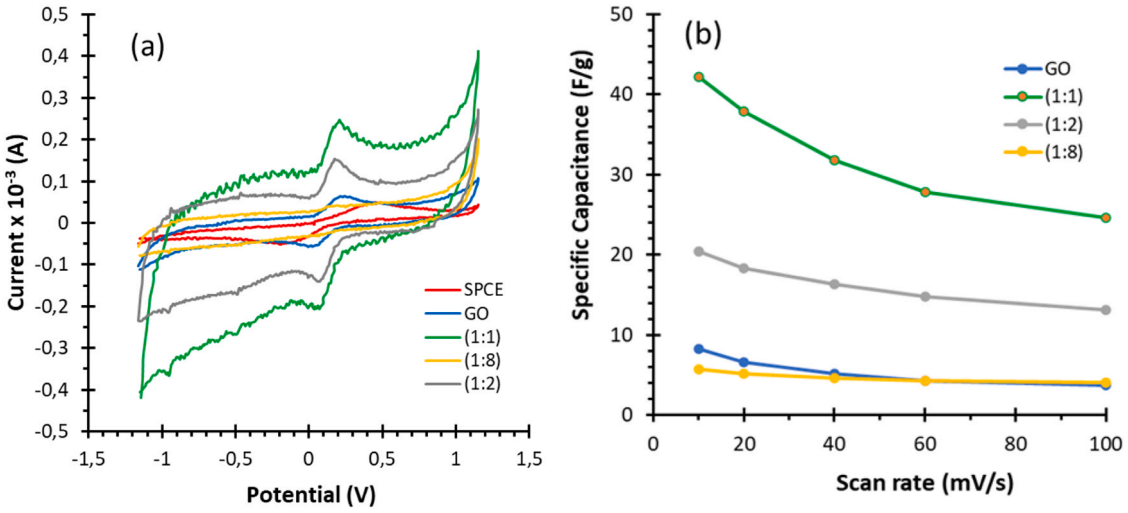

Fig. 5. (a) CV curve at 100 mV/s and (b) specific capacitance vs scan rate plot of GO and GO/ZnO-composite with 5 mmol/L $K_3[Fe(CN)_6]$ solution in 0.1 mo/L 10 mL KCl as electrolyte.

decreasing sp^2 carbon domain, which is indicated by the higher I_D/I_G ratio of the ZnO/GO composite, as shown in the 1:1 and 1:8 ratios. The insertion of ZnO in the GO caused the increasing defect in the GO/ZnO composite. As shown in Figs. 3(b) and 3(d), the peaks of the D and G bands shift and are broad, followed by an increase in the D band intensity. The broadening in the D band can be due to a disorder or defect in the samples [27]. In addition to the D and G bands, a peak corresponding to the 2D band was also observed in all the samples. The flat 2D region was observed in the ZnO/GO composite with the 1:2 and 1:8 ratios, but a sharp peak was seen in the GO and ZnO/GO composite with the 1:2 ratio. The detailed observation shown in Fig. 3(c) indicates the broadening of the 2D band and also shifts to the lower frequency region. The presence of the 2D band indicates the conversion of rGO in the GO. The results strengthen the FTIR characterisation (see Fig. 2), and the GO reduction indicates the peak at $\sim 3000\ cm^{-1}$.

The GO/ZnO composite's electrochemical properties with various composition ratios were tested using cyclic voltammetry (CV) with a 5 mmol/L $K_3[Fe(CN)_6]$ solution in 0.1 mol/L KCl as electrolyte at different potential scan rates (10, 20, 40, 60, and 100 mV/s) within a potential range of -1.2 to $+1.2$ V (see Fig. 4). KCl is the inert supporting electrolyte which ensures that the ionic strength of the solution is high and is not perturbed by the oxidation or reduction of the analyte concerned. $K_3[Fe(CN)_6]$ acts as the redox species that present the reduction peak in cyclic voltammogram [28]. The CV curves from GO and GO/ZnO with the 1:1, 1,2 and 1:8 ratios, as shown in Fig. 4(a-d), have a similar shape to the presence of a peak. The CV curves of composite don't change with scan rate, indicating excellent electrochemical stability and reversibility of the electrode. A peak was indicated an existence of redox reaction. It can be assumed as pseudo-capacitance behaviour. It is corroborated by nearly a parallelogram shape and the presence of peaks due to the influence of the pseudo-capacitance other than the faradic peak. Deviation from parallelogram shape is due to a delay while reversing the potential, ultimately coming from kinetic charging processes. It is because the charging process of the capacitor is strongly dependent on the potential. The redox peaks is attributed to formation of $[Fe(CN)_6]^{3-}$ or $[Fe(CN)_6]^{4-}$ in the charge route, and thus a reversible redox consequence happens. The redox process in the electrolyte-electrode interface is shown as follow [29],

$$[Fe(CN)_6]^{3-} + e^- \leftrightarrow [Fe(CN)_6]^{4-} \quad (1)$$

The reaction kinetics was studied by reviewing the effect of scan rate on the electrocatalytic response of the GO and GO/ZnO composites in the tested $K_3[Fe(CN)_6]$ and the results are shown in Fig. 4(a-d). It is clear that the peak oxidation current increases, while the peak oxidation potential shifts positively as the scanning rate increases from mVs^{-1} to 100 mVs^{-1}, accompanied by an increase in peak separation. In addition, the increase in scanning rate from 10 mVs^{-1} to 100 mVs^{-1} indicates that the electro-redox of the ferrocyanide ions in the GO and GO/ZnO composites is a diffusion-controlled process [30].

Detailed observation for a comparison of the CV curve area of the GO and GO/ZnO composite with the compositions of 1:1, 1:2 and 1:8 at a scan rate of 100 mV/s is shown in Fig. 5(a). The GO/ZnO with a 1:1 ratio shows the highest peak current compared to GO and the other GO/ZnO composites, which can be attributed to the synergistic effect of GO and ZnO, promoting the electron transfer between the redox probe and the electrode surface. The presence of ZnO-NRs, which were embedded in and agglomerated over the GO surface, contributes to a significant increase in peak current. The presence of ZnO-NRs acts as a defect, such as a larger plane-like edge on the ZnO-NR over the GO surface, which can be exposed for the electrolyte to provide a peak current response [31]. This result suggests that the GO/ZnO composite with a 1:1 ratio has better electrical conductivity than GO and other the CO/ZnO composites.

The GO/ZnO composite with the 1:1 ratio also exhibits a larger integrated area than the other samples. This finding reveals its superior electrochemical performance [4]. The CV curve area describes the ability to store energy in the electroactive site [32]. A larger area can store more energy compared to a smaller one. The voltammogram shows the results of the scan rate variation; the greater the scan rate, the wider the peak of the voltammogram, which shows good rate and capacitance properties [2]. Based on the voltammogram, a greater scan rate followed by a larger area of the voltammogram, shows good rate and capacitance properties.

The specific capacitance (C_s) values were calculated using the following equation [33]:

$$C_s = \frac{\int IdV}{mv\Delta V} \quad (2)$$

where ΔV is the potential window (V), m is the mass of the electroactive material (g), v is the scan rate (mV/s), while $\int IdV$ is the area of the curve on the voltammogram. The specific capacitance is proportional to the area under the CV curve. The calculated values of C_s for all samples are presented in the plot of scan rate versus specific capacitance, as shown in Fig. 5(b). The graph shows that the specific capacitance of all samples decreases with an increasing scan rate. This is because the electrolyte diffuses deep into the electrode material and interacts with the inner active sites at slow scan rates. At high scan rates, the limited

movement of the electrolytes results in just the utilisation of the outer active surface designed for charge storage [10]. Another reason is the presence of inner active sites which cannot sustain the redox reaction at low scan rates [2]. The number of sites available for the charge storage strongly influences the C_s value. The highest specific capacitance value is obtained at a scan rate of 10 mV/s, that is, 8.21, 42.23, 20.44 and 5.76 F/g for GO, and the GO/ZnO composites with compositions at ratios of 1:1, 1:2, and 1:8 respectively.

This study provides evidence that the electrochemical properties of GO/ZnO composites are strongly influenced by their microstructure. The GO/ZnO composite with a composition at the 1:1 ratio shows the best performance. This is indicated by the larger CV curve area and the higher specific capacitance than GO and the other GO/ZnO composites. The results confirm that the GO/ZnO composite with the microstructure of ZnO NRs embedded or incorporated in the GO has good electrochemical properties compared to the separated ZnO μRs or GO-ZnO or GO coated with ZnO or agglomerate GO-ZnO. The incorporation of ZnO NRs in the GO acts as electrically conductive pathways that can facilitate electron transport during the charging and discharging process [7]. Moreover, the number of mobile transport defects absorbed within the medium will affect ion mobility, which supports the charge storage capacitive behavior. A lower defect concentration obstructs ion migration within the electrolyte and increases the charge accumulation at the electrolyte-electrode interface. In the GO/ZnO composite with the microstructure separated between ZnO μRs and GO-ZnO or GO coated with ZnO, or the GO-ZnO, their microstructure causes the electrolyte contact with the material surface to decrease. This affects agglomerate the discharge and charging currents, which become less than optimal [34]. These findings suggest that GO/ZnO with the microstructure of ZnO NRs embedded or incorporated in the GO could be used for high-performance supercapacitor applications.

4. Conclusion

GO/ZnO composite was successfully synthesized using the one-pot hydrothermal technique. The results indicate that different micromorphologies of GO/ZnO composite had been produced, that is, ZnO-NRs embedded in and agglomerated over the GO surface; ZnO-uRs adhering to and separated on the GO surface; and coated ZnO on GO. The larger area of the voltammogram is shown by the GO/ZnO composite with the micromorphology of ZnO-NRs embedded in and agglomerated over the GO surface. The larger CV curve area of the voltammogram reveals the best capacitance properties.

Declaration of Competing Interest

The authors declare that they have no known competing financial interests or personal relationships that could have appeared to influence the work reported in this paper.

Acknowledgements

The research reported in this article was supported by DIPA UNNES' Applied Research program, Indonesia under grant agreement number: 401.26.4/UN37/PPK.3.1/2021.

References

[1] D. Kalpana, K.S. Omkumar, S.S. Kumar, N.G. Renganthan, A novel high power symmetric ZnO/carbon aerogel composite electrode for electrochemical supercapacitor, Electrochim. Acta 52 (2006) 1309–1315, https://doi.org/10.1016/j.electacta.2006.07.032

[2] M. Saranya, R. Ramachandran, F. Wang, Graphene-zinc oxide (G-ZnO) nanocomposite for electrochemical supercapacitor application, J. Sci: Adv. Mater. Devices 1 (2016) 454–460, https://doi.org/10.1016/j.jsamd.2016.10.001

[3] Z. Fahimi, O. Moradlou, Fabrication of ZnO@C foam: a flexible free-standing electrode for energy storage devices, Mater. Des. 189 (2020) 108525, https://doi.org/10.1016/j.matdes.2020.108525

[4] Z. Qin, Z.J. Li, G.Q. Yun, K. Shi, K. Li, B.C. Yang, ZnO nanorods inserted graphene sheets with improved supercapacitive performance, Appl. Surf. Sci. 292 (2014) 544–550, https://doi.org/10.1016/j.apsusc.2013.12.007

[5] U. Alver, A. Tanriverdi, O. Akgul, Hydrothermal preparation of ZnO electrodes synthesized from different precursors for electrochemical supercapacitors, Synth. Met.. 211 (2016) 30–34, https://doi.org/10.1016/j.synthmet.2015.11.008

[6] K.O. Otun, M.S. Xaba, S. Zong, X. Liu, D. Hildebrandt, S.M. El-Bahy, M.T. Alotaibi, Z.M. El-Bahy, ZIF-8-derived ZnO/C decorated hydroxyl-functionalized multi-walled carbon nanotubes as a new composite electrode for supercapacitor application, Colloid Interface Sci. Commun. 47 (2022) 100589, https://doi.org/10.1016/j.colcom.2022.100589

[7] K.S. Lee, C.W. Park, J.D. Kim, Synthesis of ZnO/activated carbon with high surface area for supercapacitor electrodes, Colloids Surf. A: Physicochem Eng. Asp., A 555 (2018) 482–490, https://doi.org/10.1016/j.colsurfa.2018.06.077

[8] Q. Luo, P. Xu, Y. Qiu, Z. Cheng, X. Chang, H. Fan, Synthesis of ZnO tetrapods for high-performance supercapacitor applications, Mater. Lett. 198 (2017) 192–195, https://doi.org/10.1016/j.matlet.2017.04.032

[9] D. Aryanto, E. Hastuti, M. Taspika, K. Anam, I. Isnaeni, W.B. Widayatno, A.S. Wismogroho, P. Marwoto, B.W. Nuryadin, A. Noviyanto, S. Sugianto, Characteristics and photocatalytic activity of highly c-axis-oriented ZnO thin films, J. Sol. - Gel Sci. Technol. 96 (2020) 226–235, https://doi.org/10.1007/s10971-020-05361-5

[10] S. Rai, R. Bhujel, M. Khadka, R.L. Chetry, B.P. Swain, J. Biswas, Synthesis, characterizations, and electrochemical studies of ZnO/reduced graphene oxide nanohybrids for supercapacitor application, Mater. Today Chem. 20 (2021) 100472, https://doi.org/10.1016/j.mtchem.2021.100472

[11] M. Selvakumar, D.K. Bhat, A.M. Aggarwal, S.P. Iyer, Nano ZnO-activated carbon composite electrodes for supercapacitors, G. Sravani, Phys. B 405 (2010) 2286–2289, https://doi.org/10.1016/j.physb.2010.02.028

[12] R. Sinha, N. Roy, T.K. Mandal, SWCNT/ZnO nanocomposite decorated with carbon dots for photoresponsive supercapacitor applications, Chem. Eng. J. 431 (2022) 133915, https://doi.org/10.1016/j.cej.2021.133915

[13] J. Kalaiarasi, C. Pragathiswaran, P. Subramani, Green chemistry approach for the functionalization of reduced graphene and ZnO as efficient supercapacitor application, J. Mol. Struct. 1242 (2021) 130704, https://doi.org/10.1016/j.molstruc.2021.130704

[14] T. Prabhuraj, S. Prabhu, E. Dhandapani, N. Duraisamy, R. Ramesh, K.A.R. Kumara, P. Maadeswaran, Bifunctional ZnO sphere/r-GO composites for supercapacitor and photocatalytic activity of organic dye degradation, Diam. Relat. Mater. 120 (2021) 108592, https://doi.org/10.1016/j.diamond.2021.108592

[15] N.I. Zaaba, K.L. Foo, U. Hashim, S.J. Tan, W.W. Liu, C.H. Voon, Synthesis of graphene oxide using modified Hummers method: solvent influence, Procedia Eng. 184 (2017) 469–477, https://doi.org/10.1016/j.proeng.2017.04.118

[16] A. Lerf, H. He, M. Forster, J. Klinowski, Structure of graphite oxide revisited, |, J. Phys. Chem. B 102 (1998) 4477–4482, https://doi.org/10.1021/jp9731821

[17] T.F. Emiru, D.W. Ayele, Controlled synthesis, characterization and reduction of graphene oxide: a convenient method for large scale production, Egypt. J. Basic Appl. Sci. 4 (2017) 74–79, https://doi.org/10.1016/j.ejbas.2016.11.002

[18] C.D. Zangmeister, Preparation and evaluation of graphite oxide reduced at 220 °C, Chem. Mater. 22 (2010) 5625–5629, https://doi.org/10.1021/cm102005m

[19] Z. Li, Z. Zhou, G. Yun, K. Shi, X. Lv, B. Yang, High-performance solid-state supercapacitors based on graphene-ZnO hybrid nanocomposites, Nanoscale Res. Lett. 8 (2013) 473, https://doi.org/10.1186/1556-276X-8-473

[20] R.A. Dar, G.A. Naikoo, A.K. Srivastava, I.U. Hassan, S.P. Karna, L. Giri, A.M.H. Shaikh, M. Rezakazemi, W. Ahmed, Performance of graphene-zinc oxide nanocomposite coated-glassy carbon electrode in the sensitive determination of para-nitrophenol, Sci. Rep. 12 (2022) 117, https://doi.org/10.1038/s41598-021-03495-2

[21] R. Kumar, S.M. Youssry, M.M. Abdel, G. Atsunori, One-pot synthesis of reduced graphene oxide nanosheets anchored ZnO nanoparticles via microwave approach for electrochemical performance as supercapacitor electrode, J. Mater. Sci.: Mater. Electron 31 (2020) 15456, https://doi.org/10.1007/s10854-020-04108-w

[22] M.L. de Peres, R. de Avila Delucis, S.C. Amico, D.A. Gatto, Zinc oxide nanoparticles from microwave-assisted solvothermal process: photocatalytic performance and use for wood protection against xylophagous fungus, Nanomater. Nanotechnol. 9 (2019) 1–8, https://doi.org/10.1177/1847980419876201

[23] P. Li, Z.P. Xu, M.A. Hampton, D.T. Vu, L. Huang, V. Rudolph, A.V. Nguyen, Rudolph, A.V. Nguyen, Control preparation of zinc hydroxide nitrate nanocrystals and examination of the chemical and structural stability, J. Phys. Chem. C 116 (2012) 10325–10332, https://doi.org/10.1021/jp300045u

[24] G. Nagaraju, Udayabhanu, Shivaraj, S.A. Prashanth, M. Shastri, K.V. Yathish, C. Anupama, D. Rangappa, Electrochemical heavy metal detection, photocatalytic, photoluminescence, biodiesel production and antibacterial activities of Ag–ZnO nanomaterial, Mater. Res. Bull. 94 (2017) 54–63, https://doi.org/10.1016/j.materresbull.2017.05.043

[25] K. Handore, S. Bhavsar, A. Horne, P. Chhattise, K. Mohite, J. Ambekar, N. Pande, V. Chabukswar, Novel green route of synthesis of ZnO nanoparticles by using natural biodegradable polymer and its application as a catalyst for oxidation of aldehydes, J. Macromol. Sci. Pure Appl. Chem. 51 (2014) 941–947, https://doi.org/10.1080/10601325.2014.967078

[26] R. Ramachandran, M. Saranya, P. Kollu, B.P.C. Raghupathy, S.K. Jeong, A.N. Grace, Solvothermal synthesis of Zinc sulfide decorated Graphene (ZnS/G) nanocomposites for novel Supercapacitor electrodes, Electrochim. Acta 178 (2015) 647–657, https://doi.org/10.1016/j.electacta.2015.08.010

[27] A. Kaniyoor, S. Ramaprabhu, A Raman spectroscopic investigation of graphite oxide derived graphene, AIP Adv. 2 (2012) 032183, https://doi.org/10.1063/1.4756995

[28] G. Ma, J. Li, K. Sun, H. Peng, J. Mu, Z. Lei, High performance solid-state supercapacitor with PVA–KOH–K3[Fe(CN)6] gel polymer as electrolyte and separator, J. Power Sources 256 (2014) 281–287, https://doi.org/10.1016/j.jpowsour.2014.01.062

[29] F. Yusoff, N.T. Khing, C.C. Hao, L.P. Sang, N.B. Muhamad, N.M. Saleh, The electrochemical behavior of zinc oxide/reduced graphene oxide composite electrode in dopamine, Malays. J. Anal. Sci. 22 (2018) 227–237, https://doi.org/10.17576/mjas-2018-2202-07

[30] F. Yusoff, A. Aziz, N. Mohamed, S.A. Ghani, Synthesis and characterizations of BSCF at different pH as future cathode materials for fuel cell, Int. J. Electrochem. Sci. 8 (2013) 10672–10687 ⟨http://www.electrochemsci.org/⟩.

[31] N. Rahmat, N.A. Yusof, Modification of SPCE by reduction of graphene oxide and electrodeposition of zinc oxide nanoparticles for electrochemical sensor, Malay. J. Catal. 3 (2018) 32–35 ⟨http://mjcat.utm.my/⟩.

[32] M.R. Pallavolu, J. Nallapureddy, R.R. Nallapureddy, G. Neelima, A.K. Yedluri, T.K. Mandal, B. Pejjai, S.W. Joo, Self-assembled and highly faceted growth of Mo and V doped ZnO nanoflowers for high-performance supercapacitors, J. Alloy. Compd. 886 (2021) 161234, https://doi.org/10.1016/j.jallcom.2021.161234

[33] Y.S. Choudhary, L. Jothi, G. Nageswaran, Electrochemical characterization, in: S. Thomas, R. Thomas, A.K. Zachariah, R.K. Mishra (Eds.), Spectroscopic Methods for Nanomaterials Characterization, Elsevier Inc, Netherlands, 2017, pp. 19–51.

[34] A.Y. Lo, L. Saravanan, C.M. Tseng, F.K. Wang, J.T. Huang, Effect of composition ratios on the performance of graphene/carbon nanotube/manganese oxide composites toward supercapacitor applications, ACS Omega 5 (2020) 578–587, https://doi.org/10.1021/acsomega.9b03163